ACS APPLIED MATERIALS & INTERFACES

Research Article

www.acsami.org

Mechanical Properties of Nanoporous GaN and Its Application for Separation and Transfer of GaN Thin Films

Shanjin Huang,[†,‡] Yu Zhang,[*,†] Benjamin Leung,[†] Ge Yuan,[†] Gang Wang,[‡] Hao Jiang,[‡] Yingmin Fan,[§] Qian Sun,[§] Jianfeng Wang,[§] Ke Xu,[§] and Jung Han[†]

[†]Department of Electrical Engineering, Yale University, New Haven, Connecticut 06520, United States.

[‡]State Key Laboratory of Optoelectronic Materials and Technology, Sun Yat-sen University, Guangzhou, 510275, P. R. China

[§]Suzhou Institute of Nano-Tech and Nano-Bionics (SINANO), Chinese Academy of Sciences, Suzhou, 215123, P. R. China

ABSTRACT: Nanoporous (NP) gallium nitride (GaN) as a new class of GaN material has many interesting properties that the conventional GaN material does not have. In this paper, we focus on the mechanical properties of NP GaN, and the detailed physical mechanism of porous GaN in the application of liftoff. A decrease in elastic modulus and hardness was identified in NP GaN compared to the conventional GaN film. The promising application of NP GaN as release layers in the mechanical liftoff of GaN thin films and devices was systematically studied. A phase diagram was generated to correlate the initial NP GaN profiles with the as-overgrown morphologies of the NP structures. The fracture toughness of the NP GaN release layer was studied in terms of the voided-space-ratio. It is shown that the transformed morphologies and fracture toughness of the NP GaN layer after overgrowth strongly depends on the initial porosity of NP GaN templates. The mechanical separation and transfer of a GaN film over a 2 in. wafer was demonstrated, which proves that this technique is useful in practical applications.

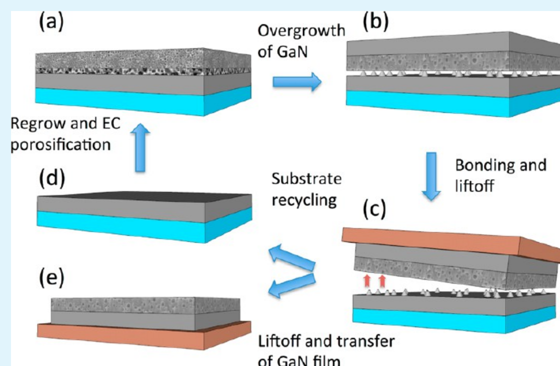

KEYWORDS: *nanoporous GaN, mechanical properties, layer separation and transfer*

1. INTRODUCTION

GaN has become one of the most important semiconductors with wide applications in solid-state lighting and power electronics.[1,2] However, high mechanical strength and chemical inertness of GaN brings extra challenges in device fabrication, micromachining and layer separation. GaN and GaN based optoelectronics devices are primarily grown on sapphire, which limits the performance of devices because of their poor thermal and electrical conductivity.[3] Removal of the sapphire substrate allows the fabrication of vertical devices and gives flexibility in optimizing current spreading, thermal management and light extraction.[4] The most common method to separate GaN from sapphire substrates is the ultraviolet (UV) laser-liftoff (LLO) technique.[5] However, LLO is limited by the requirement of deep-UV transparent substrates; it cannot be applied to non-UV transparent substrates like Si, SiC, and bulk GaN. Alternative methods are being explored, including chemical liftoff by etching of sacrificial layers,[6−9] and mechanical liftoff via a release layer such as graphene and BN.[10−12]

Recently, the fabrication of nanoporous (NP) GaN by an electrochemical etch was reported.[13,14] Because of its high surface-to-volume ratio, NP GaN shows significantly different behaviors in mechanical properties, chemical inertness and thermal stability compared to the conventional GaN material. One interesting prospect of NP GaN is the potential reduction of elastic modulus, hardness and fracture toughness because of the porous structures. In our previous study, NP GaN was proposed as an alternative liftoff technique with a proof-of-concept demonstration of a vertical LED.[15] The study was mostly empirical because of the absence of quantitative information regarding the mechanical and microstructural properties of NP GaN, such as porosity, adhesion, and fracture toughness. A quantitative and comprehensive study of the mechanical properties of the NP GaN pertaining to layer separation is thereby required.

In this paper, we focus on the mechanical properties of NP GaN, and the detailed physical mechanism of porous GaN in the application of liftoff. First, we studied the mechanical properties of NP GaN by using a nanoindentation technique. The values of elastic modulus and hardness of NP GaN were achieved, with a trend of decreasing monotonically with an increase in the porosity of NP GaN. Then, the application of the NP GaN as a release layer to epitaxial liftoff of GaN films was systematically studied. According to the correlation of the initial porous profiles of NP GaN templates with their as-overgrown morphologies, a phase diagram was generated to analyze the shape transformation of NP GaN. The fracture toughness of the NP GaN release layers was investigated and

Received: August 8, 2013
Accepted: October 14, 2013
Published: October 14, 2013

© 2013 American Chemical Society

dx.doi.org/10.1021/am4032345 | ACS Appl. Mater. Interfaces 2013, 5, 11074−11079

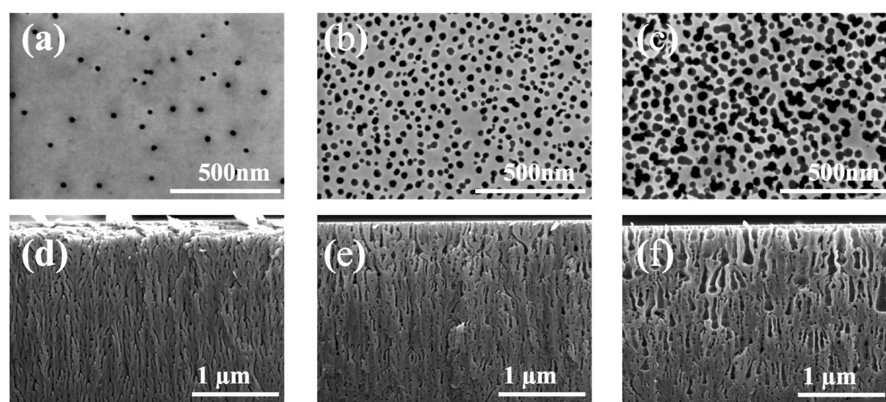

Figure 1. (a−c) Top view and (d−f) cross-sectional SEM images of NP GaN with different porosity etched at (a, d) 10, (b, e) 15 and (c, f) 20 V, respectively.

correlated with the voided-space-ratio. By optimizing initial porous GaN profile, we developed a technological process to control the fracture toughness of the NP release layer, which gives a useful guideline for the proposed liftoff process. Finally, the separation and transfer of a GaN film over a 2 in. sapphire wafer was demonstrated. The scale-up of transferred GaN film to 2 in. diameter proves that this technique is useful in practical applications.

2. EXPERIMENTAL SECTION

NP GaN was created by applying electrochemical etching (EC) on a Si-doped n-GaN according to a procedure reported recently.[13] Si-doped n-GaN was grown by metal−organic chemical vapor deposition (MOCVD).[16] Oxalic Acid with a concentration of 0.3 M was used as the electrolyte for EC porosification. The GaN sample and a platinum wire are used as anode and cathode, respectively. An Anodic voltage was applied to the GaN sample using voltage-controlled mode during the etching. By adjusting the anodic voltages and Si-doped level of n-GaN, NP GaN with different porosities (ρ) from ∼10% (sparse distribution of pores) up to ∼70% (dense and coalesced pores by electropolishing) can be achieved.[14] Three NP GaN samples with a thickness of 2 μm were prepared for nanoindentation test by EC etching at 10, 15, and 20 V, respectively. To incorporate the NP GaN into the proposed epitaxial liftoff method, we employed an optimized designed two-layer NP GaN profile. The two-layer NP GaN is with a low porosity (LP) NP GaN on top and a high porosity (HP) NP GaN layer at the bottom (Figure 3a), which was achieved by first EC etching a n-GaN ($n = 2 \times 10^{19}$ cm^{-3}) at a low voltage followed by a high voltage etching. The LP layer on top serves as a homoepitaxy-like nucleation layer for overgrowing high quality GaN films while the HP layer at the bottom serves as the release layer for separation. The thickness of LP GaN is around 600 nm and its porosity is ρ = 15%. The thickness of HP GaN varies from 50 to 600 nm while the porosity varies from ρ = 45% to ρ = 65% by controlling the EC porosification time and the anodic voltage, respectively. After cleaning, the NP GaN was reloaded into a MOCVD reactor for the overgrowth of 4 μm GaN at 1030 °C. The morphology of the samples was characterized using scanning electronic microscopy (SEM, Hitachi SU-70) and Nomarski optical microscopy. The mechanical properties of the as-etched NP GaN were characterized by nanoindentation tests using an Agilent Nano Indenter G200.

3. RESULTS AND DISCUSSION

A. Mechanical Properties of NP GaN. Figure 1 shows the top view and cross sectional SEM images of three NP GaN samples. The porosity of NP GaN increases with applied bias increasing. The porosity (ρ) of the three NP GaN are (a, d) 18, (b, e) 25, and (c, f) 45% for, respectively, which were estimated from the cross sectional SEM images. Under a low bias, EC porosification begins preferentially around the dislocations on the GaN surface. During the EC porosification, the oxidation and dissolution of GaN occur selectively near the tips of the pore.[14,15,17] The pores then extend generally following the electrical fields or the directions of currents as seen in Figure 1d−f.

It is known that porosity has a considerable effect on the mechanical properties, and nanoindentation technique has been used to study the mechanical properties of porous materials.[18,19] In nanoindentation measurements, the displacements of NP GaN during the loading phase involve both elastic and plastic mechanisms, while only elastic behavior exists during the unloading phase. The load−displacement curves of the three NP GaN with a reference sample (ρ = 0%) are shown in Figure 2a. The peak displacement of NP GaN increases with increasing of the porosity, from 223 nm for reference GaN to 351 nm for NP GaN with ρ = 45%, which implies the decrease in the elastic modulus and hardness of porous GaN. And elastic modulus and hardness can be extracted from the load−displacement curves.[20] Figure 2b gives the trend of elastic modulus and hardness of NP GaN as a function of porosity. The elastic modulus decreases from 361 GPa for reference GaN film to 193 GPa for NP GaN with ρ = 45% (decrease by 46%), whereas the hardness decreases at the same time from 14.3 to 7.1 GPa (decreases by 63%). It can be observed that the elastic modulus and hardness is significantly lower for high porosity GaN than that of GaN. Thus, such porous GaN layers appeared mechanically fragile to be used as a release layer for the applications of layer separation and transfer.[18,21]

B. Application of NP GaN on Epitaxial Liftoff. The basic concept of the epitaxial liftoff method is illustrated in Figure 3. The process started from the porosification of GaN followed by high temperature GaN overgrowth on it. Spontaneous reorganization of NP GaN occurs during the high-temperature (∼1000 °C) overgrowth of GaN in MOCVD. This shape reorganization of pores in NP GaN is driven by Rayleigh instabilities and surface diffusion in order to reduce the total surface energy, in which the cylindrical pores formed by EC etching will transfer to elliptic voids, as shown in Figure 4d. This shape-transformation of NP GaN during overgrowth is a critical process for the liftoff. However, it is not clear that how do the shape transformation and fracture toughness of the NP GaN release layer depend on the initial porous GaN profiles for layer separation applications. Therefore, a systematic study on

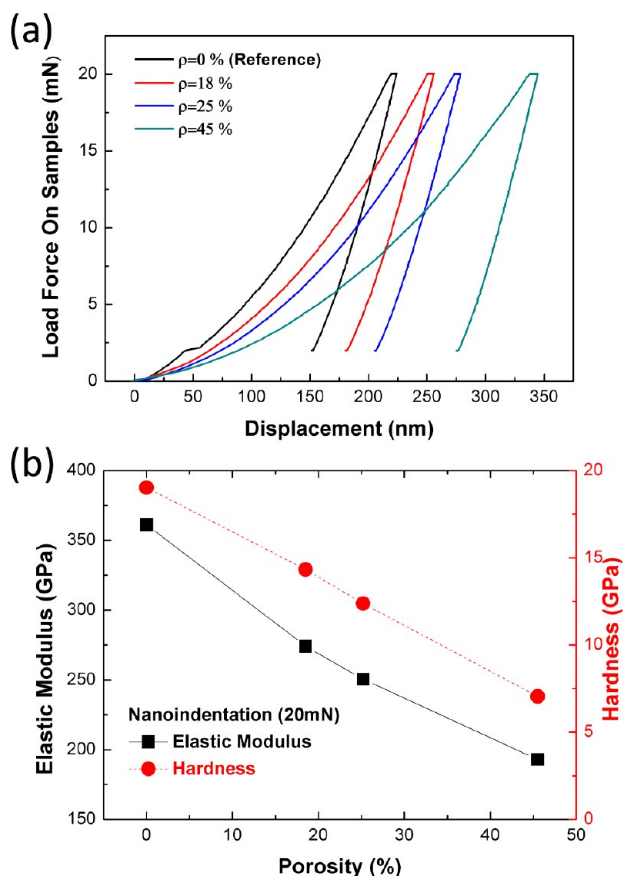

Figure 2. (a) Load−displacement curves of the as-etched NP GaN with various porosities. (b) Elastic modulus and hardness as a function of porosity of NP GaN.

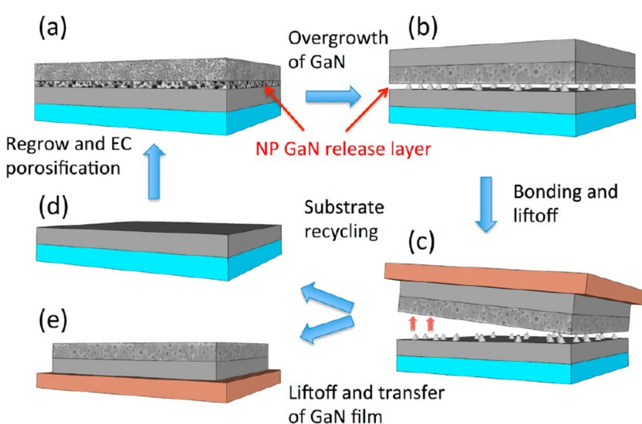

Figure 3. Sketch of the concept of the liftoff process incorporating NP GaN as a release layer. (a) Preparation of a porous GaN with optimized two-layer porosity profile; (b) MOCVD overgrowth of GaN on NP GaN templates; (c) wafer bonding to the overgrown GaN thin film; (d) Recycling of substrates/templates; (e) separation and transfer of large-area GaN thin film onto other substrates/carriers.

controlling both the transformation and fracture toughness of the NP GaN release layer is carried out.

Figure 4a−c and d−f show the morphologies of as-etched NP GaN and their corresponding shape transformation after the overgrowth, respectively. For NP GaN with an initial porosity of ρ = 45% (Figure 4a), the porous structure transformed into discrete voids with diameters around ∼1 μm after GaN overgrowth on it. These transformed voids are separated from several hundred nanometers to several micrometers (Figure 4d). For this initial porosity (ρ = 45%), the fracture toughness of NP layer is too large to separate overgrowth GaN layer. When we increased the porosity to ρ = 55% (Figure 4b), the initial transformation was followed by the coalescence and expansion of voids, analogous to the coalescence of pores in Si due to mass transport.[22,23] As a result, the morphology of large voided space with pillars (diameter <500 nm) is formed as seen in Figure 4e. Thus, the fracture toughness of the NP layer is sufficiently small to mechanically release the overgrowth GaN layer. When we further increased the porosity to above a sufficiently high porosity (ρ = 65%)(Figure 4c), a large airgap was obtained (Figure 4f). The different morphologies of the NP structure after overgrowth can also be distinguished from the Nomarski optical microscopy images as shown in Figure 4g−i. The bright white regions represent the voided space in the NP GaN whereas the green (or dark) regions are the residual GaN sidewalls/pillars connecting the overgrowth layer. It can be observed that some individual small dots (Figure 4g) and large area voids (Figure 4h, i) were produced from low and high porosity layers during high temperature growth, respectively. The interesting morphologies of NP GaN are schematically drawn in Figure 4j−l for clearer understanding. The blue regions represent the residual GaN in the NP GaN release layer, whereas the white regions represent the voided space in the release layer. With increasing the initial porosity in the lower HP GaN layer, the area of residual GaN in NP GaN release layer (blue region) shrinks gradually, resulting in the different morphologies.

To quantify the shape-transformation of the NP GaN release layer, we generated an empirical phase diagram (Figure 5) to correlate between the initial porosity and thickness and the transformed morphologies of the NP GaN layer after overgrowth. We found that both the initial porosity and thickness of the HP GaN layer can affect the transformed morphology after overgrowth. This phase diagram can be divided into three regimes (I, II, and III). After overgrowth process, NP GaN with a low porosity or small thickness in regime I (ρ < 50%, t < 100 nm) will transform into the discrete-voids morphology, similar to that in panels d and g in Figure 4; NP GaN with a higher porosity and thickness in regime II (50% < ρ < 60%, 200 nm < t < 400 nm) will transform into large voided space with pillars, similar to that in panels e and h in Figure 4, whereas NP GaN with excessively high porosity and thickness in regime III (ρ>60%, t > 400 nm) will form a large airgap, similar to that in panels f and i in Figure 4. In general, the porosity influences the shape transformation of NP GaN more strongly than the thickness does, as indicated by the logarithmic scale of the y-axis in Figure 5.

It is worth noting that a complete airgap in the proposed liftoff method is not always preferable. A low density of connecting pillars makes the overgrown GaN membrane very fragile and susceptible to uncontrolled peel-off. Also, the pronounced transformation to a large air-gap (regime III) results in excessive amount of liquid gallium droplets, which may deteriorate the crystalline quality of the overgrown GaN due to the catalytic etching by Ga droplets.[24,25] The preferred initial porosity-thickness-profile of NP GaN for liftoff should be within the window of regime II with proper bonding.

Three kinds of bonding materials: Copper tape (3 M #1182 HD), Silver epoxy (MG chemicals, No.8331−14g) and Devcon

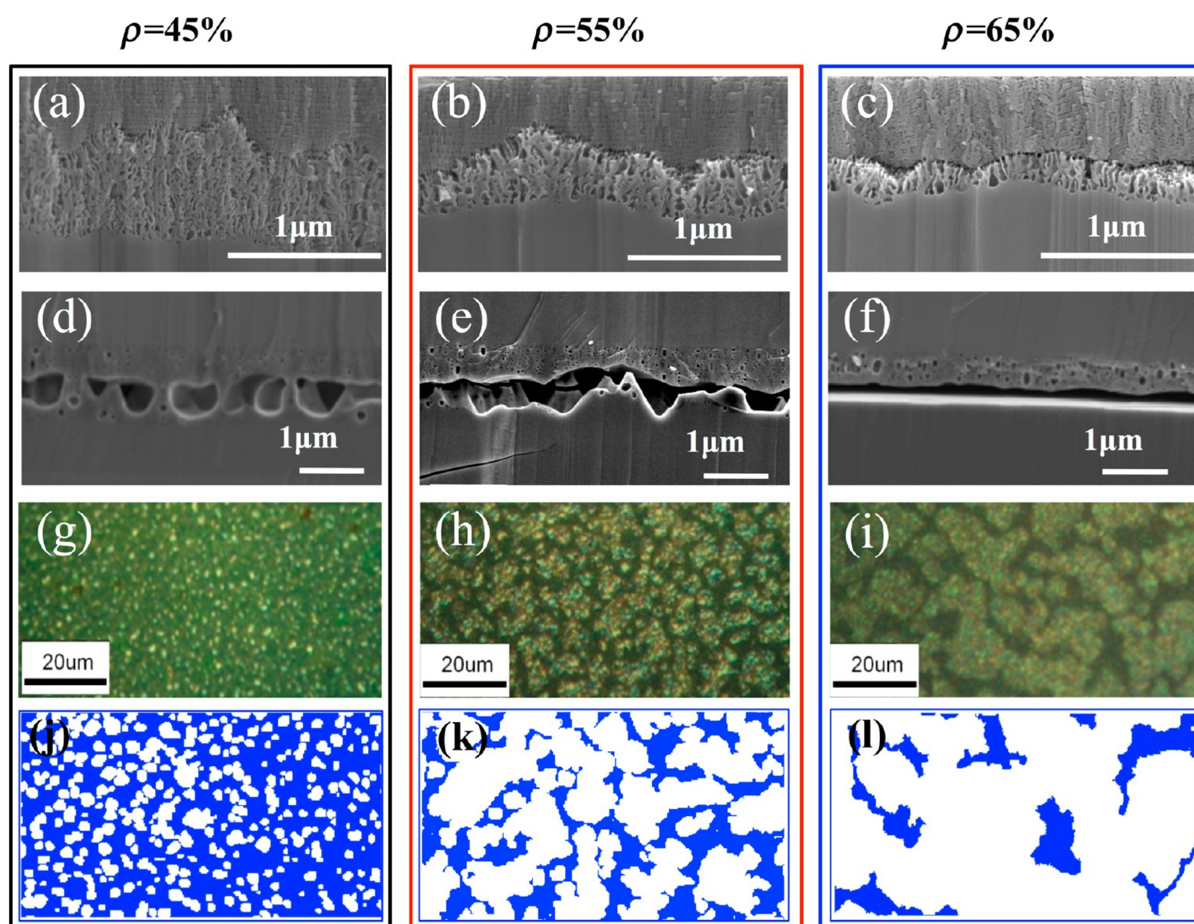

Figure 4. Shape transformation of the NP GaN release layers with different porosity: ρ = 45, 55, and 65% (porosities were estimated using cross-sectional SEM images). (a−c) Cross-sectional SEM images of the as-etched porous GaN templates with different porosity in the bottom high porosity layer. The low-porosity layers on top in a−c are ρ = 15%. (d−f) Corresponding cross-sectional SEM images after overgrowing 4 μm GaN on NP GaN, showing the different shape transformation morphologies: (d) discrete voids, (e) large voided space with pillars, and (f) a large airgap. (g−i) Top-view Nomarski optical microscopy images of the overgrown GaN. (j−l) Schematic drawings of the transformed NP GaN structures extracted from the Nomarski images.

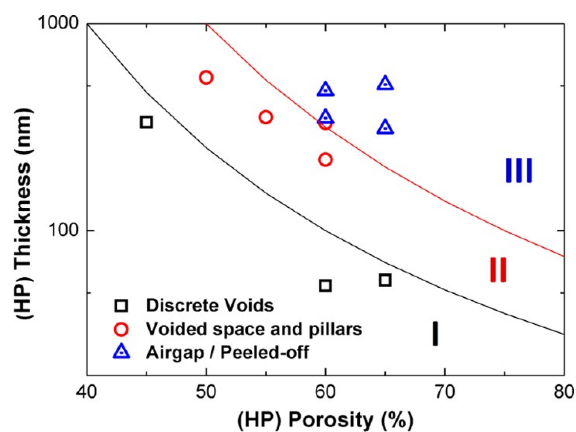

Figure 5. A "phase diagram" of the as-etching NP-GaN profile to correlate the initial porosity and thickness to the transformed morphology of the NP GaN release layer after overgrowth. Three regimes represent different as-overgrowth morphologies are defined.

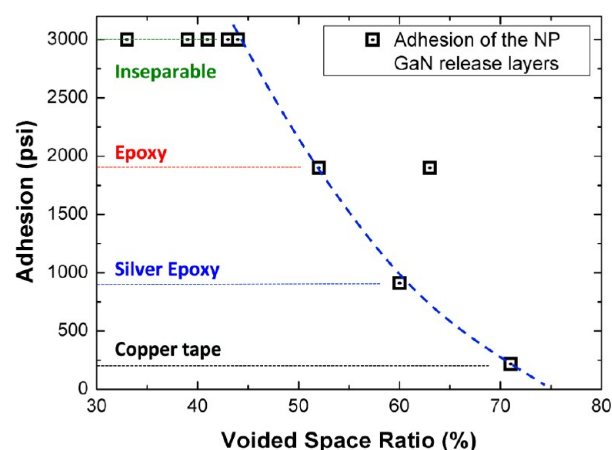

Figure 6. Adhesion of the bonding materials with various voided-space-ratio after GaN overgrowth. A boundary cure (dashed blue line) of the separable region (up-right region) is roughly defined. Samples that could not be separated even by epoxy were treated inseparable and set to have an adhesion of 3000 psi in the figure. The horizontal dotted lines indicate the adhesion of three bonding materials used in the study.

ev-Tube epoxy (Devcon, S-208/20845) were used for separating the overgrown GaN films. The adhesion of these three bonding materials are given by product datasheets and indicated in Figure 6. A Plot to correlate the voided-space-ratio

dx.doi.org/10.1021/am4032345 | ACS Appl. Mater. Interfaces 2013, 5, 11074−11079

after overgrowth and adhesion of bonding materials was generated in Figure 6. The voided-space-ratio is defined as: the voided-space-area/total-area, which was extracted from the Nomasiki images (the area of bright white regions/the total area in Figure 4g–i. We use the adhesion of bonding materials to demarcate the fracture toughness of NP GaN. For example, a sample with 50% voids can be separated with epoxy but not sliver epoxy, thus placing its interface adhesion strength with an upper bond of the strength of epoxy adhesion. NP GaN with a high voided-space-ratio of 70% acts very well as mechanical release layer to release the overgrown GaN films even just using copper tapes. NP GaN with a voided-space-ratio <40% cannot serve as release layers for separation in our experiments. The separable region located on the up-right of Figure 6 is defined by the blue dashed boundary curve. The actual value of the stress of NP GaN could be smaller than those indicated in the blue dashed curve, otherwise the separation will occur at the interfaces of the bonding materials and the samples. Using bonding materials with stronger adhesion can further extend the separable region to the NP GaN with lower voided-space-ratio.[26] It is worth noting that Figure 6 is the first quantitative measurement/estimation of the stress regard to separate NP GaN as a function of porosity, which can be further used to estimate the important mechanical property of NP GaN-fracture toughness.

The fracture toughness of porous GaN was extracted by the following equation using a compact tension specimen[27]

$$K = 1.12\sigma\sqrt{\pi a} \quad (1)$$

Where K is the fracture toughness, σ is the applied stress, a is the crack length or void size. The stress of the NP GaN extracted from Figure 6 was used for σ, and the largest void in the porous GaN layer was used for a. The values estimated based this model are listed in Table 1. It can be observed that

Table 1. Summary of the Estimated Fracture Toughness of Porous GaN Layers

voided space ratio p (%)	fracture toughness $K = 1.12\sigma(\pi a)^{1/2}$(Mpa$\sqrt{m}$)	m
0	0.8[30]	
50	0.0450	4.15
60	0.0390	3.29
70	0.0127	3.44

the fracture toughness decreases with increasing of porosity, because the net loading area in porous structure would be subjected to higher stresses compared with a less porous GaN under the same load, and increased porosity would also introduce additional stress concentrations. To further confirm the estimation, an empirical dependence of K/K_0 on porosity reported in porous ceramics is used[28,29]

$$K = K_0(1 - p)^m \quad (2)$$

Where K and K_0 are the fracture toughness of porous material and porous-free material, respectively, p is the porosity, and m depends on the pore shape and pore size in the range 2–5. We applied this model to GaN material using K_0 = 0.8 MPa$\sqrt{m}$[30] and voided-space ratio (p) of porous GaN layer as shown in Figure 6. The deduced m are also shown in table 1. This model applies quite well to the porous GaN films. The results are consistent with our experiment that higher porosity of porous GaN layer has smaller fracture toughness, which is easier to separate.

Figure 7 shows an optical image of a 4 μm thick 2 in. GaN film transferred on to a copper carrier (right) using the optimized NP GaN profiles and epoxy bonding. The transferred GaN film is crack-free over 2″ wafer under the Nomarski optical microscopy. The template (here is sapphire) after liftoff can be recycled for starting a new liftoff cycle, as shown in Figure 3a–d, which is particularly valuable for expensive substrates like bulk GaN.[31] The carrier wafer for the liftoff GaN film is not necessary to be copper. GaN on flexible substrates[32] and amorphous glass[33] are also possible for the proposed liftoff process, which can even create more potentiality in various applications.

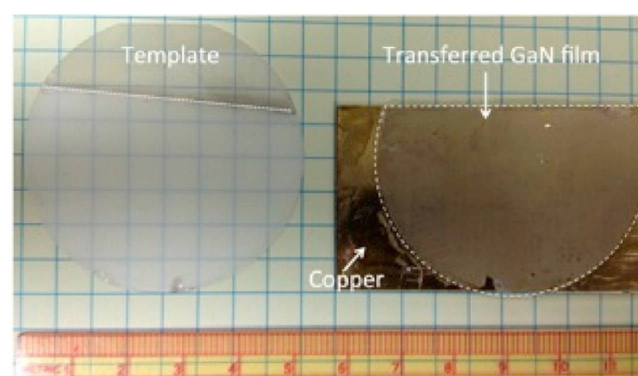

Figure 7. Optical image of a 2 in. GaN film transferred on to a copper carrier (right) using the proposed liftoff method incorporating NP GaN and the template (left) after GaN liftoff. The transferred GaN thin film is indicated by the white dashed circle. The region under the white dashed line in the template is the porosified region while the upper region is for electrical contact during EC etching.

4. CONCLUSION

The mechanical property of the NP GaN was studied. Obvious reduction of the elastic modulus and hardness of NP GaN compared to the conventional GaN film was identified by using a nanoindentation technique. The epitaxial liftoff process incorporating the NP GaN material as a release layer was systematically investigated through the starting porosity profile of the NP GaN release layer to the shape transformation as well as the fracture toughness after overgrowth. Finally, we demonstrated the separation and transfer of a GaN thin film over a 2 in. wafer using the proposed process. We believe this NP GaN material and the proposed epitaxial liftoff process will open the potential of the heterogeneous integration of GaN-based electronics with a variety of host materials.

■ AUTHOR INFORMATION

Corresponding Author

*E-mail: yu.zhang@yale.edu.

Notes

The authors declare no competing financial interest.

■ ACKNOWLEDGMENTS

This work was supported by National science foundation (NSF) under Award No. CMMI-1129964, and Facilities used were supported by Yale Institute for Nanoscience and Quantum Engineering and NSF MRSEC DMR 1119826.

Jung Han acknowledges research support and financial interest in Seoul Optodevice. Shanjin Huang acknowledges support from China Scholarship Council (CSC).

REFERENCES

(1) Tsao, J. Y.; Coltrin, M. E.; Crawford, M. H.; Simmons, J. A. *Proc. IEEE* **2010**, *98*, 1162−1179.
(2) Okumura, H. *Jpn. J. Appl. Phys.* **2006**, *45*, 7565−7586.
(3) Huang, S.; Wu, H.; Fan, B.; Zhang, B.; Wang, G. *J. Appl. Phys.* **2010**, *107*, 054509.
(4) Wang, S. J.; Uang, K. M.; Chen, S. L.; Yang, Y. C.; Chang, S. C. *Appl. Phys. Lett.* **2005**, *87*, 011111.
(5) Wong, W. S.; Sands, T.; Cheung, N. W. *Appl. Phys. Lett.* **1998**, *72*, 599−601.
(6) Watson, I. M.; Liu, C.; Gu, E.; Dawson, M. D.; Edwards, P. R.; Martin, R. W. *Appl. Phys. Lett.* **2005**, *87*, 151901.
(7) Rogers, D. J.; Teherani, F. H.; Ougazzaden, A.; Gautier, S.; Divay, L.; Lusson, A.; Durand, O.; Wyczisk, F.; Garry, G.; Monteiro, T.; Correira, M. R.; Peres, M.; Neves, A.; McGrouther, D.; Chapman, J. N.; Razeghi, M. *Appl. Phys. Lett.* **2007**, *91*, 071120.
(8) Ha, J.-S.; Lee, S. W.; Lee, H.-J.; Lee, H.-J.; Lee, S. H.; Goto, H.; Kato, T.; Fujii, K.; Cho, M. W.; Yao, T. *IEEE Photonics Technol. Lett.* **2008**, *20*, 175−177.
(9) Park, J.; Song, K. M.; Jeon, S.-R.; Baek, J. H.; Ryu, S.-W. *Appl. Phys. Lett.* **2009**, *94*, 221907.
(10) Zang, K. Y.; Cheong, D. W. C.; Liu, H. F.; Liu, H.; Teng, J. H.; Chua, S. J. *Nanoscale Res. Lett.* **2010**, *5*, 1051−1056.
(11) Chung, K.; Lee, C.-H.; Yi, G.-C. *Science* **2010**, *330*, 655−657.
(12) Kobayashi, Y.; Kumakura, K.; Akasaka, T.; Makimoto, T. *Nature* **2012**, *484*, 223−227.
(13) Zhang, Y.; Ryu, S. W.; Yerino, C.; Leung, B.; Sun, Q.; Song, Q.; Cao, H.; Han, J. *Phys. Status Solidi B* **2010**, *247*, 1713−1716.
(14) Zhang, Y.; Sun, Q.; Leung, B.; Simon, J.; Lee, M. L.; Han, J. *Nanotechnology* **2011**, *22*, 045603.
(15) Zhang, Y.; Leung, B.; Han, J. *Appl. Phys. Lett.* **2012**, *100*, 181908.
(16) Han, J.; Ng, T. B.; Biefield, R. M.; Crawford, M. H.; Follstaedt, D. M. *Appl. Phys. Lett.* **1997**, *71*, 3114−3116.
(17) Chen, D.; Xiao, H.; Han, J. *J. Appl. Phys.* **2012**, *112*, 064303.
(18) Stragier, A.-S.; Signamarcheix, T.; Salvetat, T.; Nolot, E.; Dechamp, J.; Mercier, D.; Gergaud, P.; Tauzin, A.; Clavelier, L.; Lemiti, M. *J. Electrochem. Soc.* **2011**, *158*, H595−H599.
(19) Bellet, D.; Lamagnère, P.; Vincent, A.; Bréchet, Y. *J. Appl. Phys.* **1996**, *80*, 3772−3774.
(20) Oliver, W. C.; Pharr, G. M. *J. Mater. Res.* **1992**, *7*, 1564−1583.
(21) Joshi, M. B.; Goorsky, M. S. *J. Appl. Phys.* **2010**, *107*, 024906.
(22) Mizushima, I.; Sato, T.; Taniguchi, S.; Tsunashima, Y. *Appl. Phys. Lett.* **2000**, *77*, 3290−3292.
(23) Sudoh, K.; Iwasaki, H.; Hiruta, R.; Kuribayashi, H.; Shimizu, R. *J. Appl. Phys.* **2009**, *105*, 083536.
(24) Schoonmaker, R. C.; Buhl, A.; Lemley, J. *J. Phys. Chem.* **1965**, *69*, 3455−3460.
(25) Haino, M.; Yamaguchi, M.; Miyake, H.; Motogaito, A.; Hiramatsu, K.; Kawaguchi, Y.; Sawaki, N.; Iyechika, Y.; Maeda, T. *Jpn. J. Appl. Phys.* **2000**, *39*, L449−L452.
(26) Schmidt, M. A. *Proc. IEEE* **1998**, *86*, 1575−1585.
(27) Gdoutos, E. E. *Fracture Mechanics: An Introduction*, 2nd ed.; Springer: Amsterdam, The Netherlands, 2005; p 53.
(28) Wagh, A. S.; PLSign, J.; Poeppel, R. B. *J. Mater. Sci.* **1993**, *28*, 3589.
(29) Boccaccini, A. R. *J. Mater. Sci. Lett.* **1997**, *16*, 683.
(30) Drory, M. D.; Ager, J. W.; Suski, T.; Grzegory, I.; Porowski, S. *Appl. Phys. Lett.* **1996**, *69*, 4044−4046.
(31) Nishida, T.; Saito, H.; Kobayashi, N. *Appl. Phys. Lett.* **2001**, *79*, 711−713.
(32) Park, S. I.; Le, A. P.; Wu, J.; Huang, Y.; Li, X.; Rogers, J. A. *Adv. Mater.* **2010**, *22*, 3062−3066.
(33) Choi, J. H.; Zoulkarneev, A.; Kim, S. I.; Baik, C. W.; Yang, M. H.; Park, S. S.; Suh, H.; Kim, U. J.; Son, H. B.; Lee, J. S.; Kim, M.; Kim, J. M.; Kim, K. *Nat. Photonics* **2011**, *5*, 763−769.